NUMERICAL SIMULATION OF FLOW OVER A BACKWARD FACING STEP USING FOURIER PSEUDO-SPECTRAL METHOD COUPLED WITH IMMERSED BOUNDARY METHOD

Felipe Pamplona Mariano, fpmariano@mecanica.ufu.br
Universidade Federal de Goiás - UFG, Escola de Engenharia Elétrica e de Computação - EEEC, Goiânia - GO
Leonardo de Queiroz Moreira, lqmoreira@mecanica.ufu.br
Aristeu da Silveira Neto, aristeus@mecanica.ufu.br
Universidade Federal de Uberlândia - UFU, Faculdade de Engenharia Mecânica - FEMEC, Laboratório de Mecânica dos Fluidos - MFLab, Av. João Naves de Avilla, 2121, Campus Santa Mônica, Bloco: 5P, Uberlândia - MG

Abstract. The Immersed Boundary Method (IBM) have been widely used in Computational Fluids Dynamic (CFD) for simulating flows over complex geometries. IBM represents the boundary conditions through a force field imposed at Navier-Stokes equations. Nevertheless it presents, generally, low accuracy and low convergence rate. Aiming to solve this restriction, a new methodology is proposed at the present work, which uses the Pseudo-Spectral Fourier Method. This method provides an excellent numerical accuracy, and with the development of the Fast Fourier Transform algorithm (FFT), it presents a low computational cost in comparison with another high-accuracy methods. Another important issue is the projection method for incompressible Navier-Stokes equations. In Fourier space, this procedure does not require to solve a Poisson equation, which is usually the most computational onerous part in classical methodologies. In order to validate the new methodology it was proposed to simulate a CFD classical problem: the two and three dimensional backward-facing step flow.

Keywords: Computational Fluids Dynamic, Fourier Pseudo-Spectral Method, Immersed Boundary Method, Flow over a Circular Cylinder, Flow over a Backward-Facing Step

1. INTRODUCTION

This geometry is widely used to validate new methodologies due to its geometrical simplicity and the high control of detachment point of boundary layer of expansion. On the other hand, the flow developed downstream the expansion is very complex. A large number of experimental (Lee and Mateescu, 1998; Armaly *et al.*, 1983; Eaton and Johnston, 1980) and numerical (Gartling, 1990; Silveira-Neto *et al.*, 1993; Le *et al.*, 1997) studies has been carried out.

Figure 1 shows the global physical features expected for this problem and Fig. 2 shows the geometrical characteristics. The geometry shown in Fig. 1 is a channel of entry length with L_{in} and width $(W - h)$. The step has a height h and the exit channel has a length L and width W. The ratio W/h is named aspect ratio.
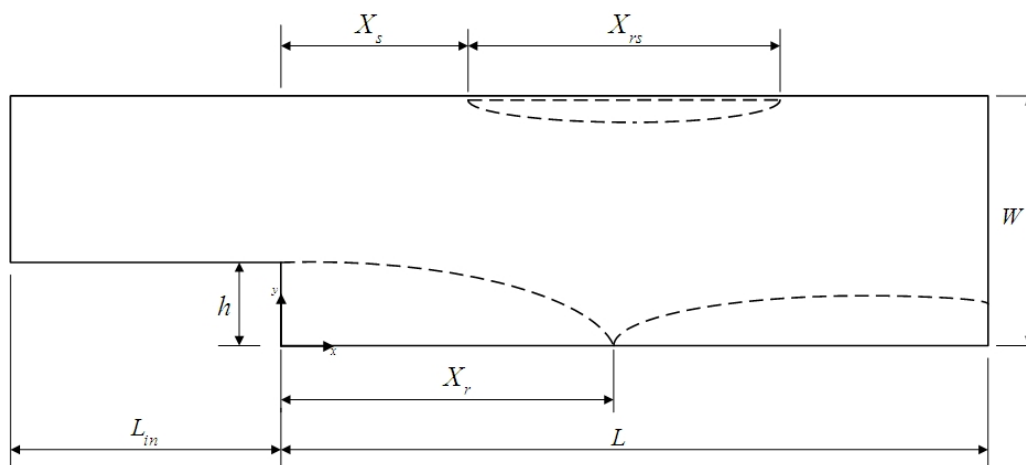

Figure 1. Backward facing step: geometrical characteristics.

In Fig. 2 the flow goes from left to right. The lower boundary layer detach in expansion point $(0, h)$. Independent of upstream flow the detachment point does not change its position. After this point, a shear layer arises. It is characterized by inflectional mean velocity field, appearing Kelvin-Helmholtz instabilities $(K - H)$. This instabilities are carried and collisions occurs over inferior wall in a particular point, named reattachment point, displayed in Fig. 1 as X_r.

Normally this flow is unsteady and therefore the reattachment point must be statistically determined. The $K - H$ in-

stabilities that make collisions against the bottom wall can be transported to the outlet or can be retained into recirculation, left of the reattachment point.
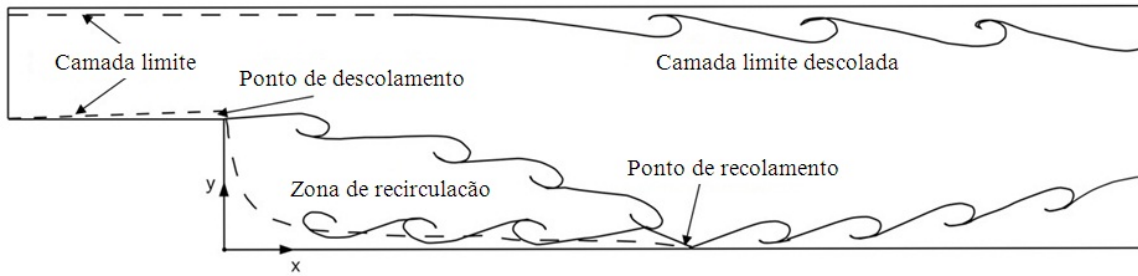

Figure 2. Backward facing step: global physical features.

After the reattachment point there are strong interactions among $K - H$ eddies and the walls. On the other hand, in the flow through an expansion there is a pressure drop, which is recovered through the outlet channel. So there is an adverse gradient pressure and the superior boundary layer detaches. This fact yields instabilities in the upper wall vicinity. The interactions of instabilities with the walls yield counter-clockwise vortex which travel through the channel. Vortex created in one wall interacts with the opposite wall.

The main characteristic of this problem is that the geometry is very simple, but the flow inside it is very complex, where one can found physical instabilities of several natures, like boundary layer, Kelvin-Helmholtz, collision of instabilities with the walls, interaction between them, boundary layer detachments, boundary layer reattachments and boundary layer and Kelvin-Helmholtz interaction. The interaction of Kelvin-Helmholtz instabilities with walls creates counter-rotating pairs that can cross the entire channel, going from a wall to the opposite one. Therefore, this geometry results a very complex and interesting benchmark to validate a new methodology.

2. MATHEMATICAL MODELING

In this section the mathematical model of immersed boundary method, based in Multi-Direct Forcing presented by Wan and Turek (2007) is presented. After that, the equations which govern the problem will be transformed to Fourier spectral space are also presented, finally the methodology proposed in this paper, is verified.

2.1 Mathematical model for the fluid

The flow is governed by momentum equation (Eq. 1) and the continuity equation (Eq. 2). These equations are solved in the domain Ω shown in Fig. 3. The information of the fluid/solid interface (domain Γ) is passed to eulerian domain (Ω) for addition of the source term to Navier-Stokes equations. The source term represents the boundary conditions of the immersed geometry as a body force (Goldstein *et al.*, 1993). The equations that govern the problem are presented in theirs tensorial form:

$$\frac{\partial u_i}{\partial t} + \frac{\partial (u_i u_j)}{\partial x_j} = -\frac{\partial p}{\partial x_i} + \nu \frac{\partial^2 u_i}{\partial x_j \partial x_j} + f_i, \tag{1}$$

$$\frac{\partial u_j}{\partial x_j} = 0, \tag{2}$$

where $\frac{\partial p}{\partial x_i} = \frac{1}{\rho}\frac{\partial p*}{\partial x_i}$; $p*$ is the static pressure in $[N/m^2]$; u_i is the velocity in i direction in $[m/s]$; $f_i = \frac{f_i^*}{\rho}$; f_i is the term source in $[N/m^3]$; ρ is the density; ν is the cinematic viscosity in $[m^2/s]$; x_i is the spatial component (x, y) in $[m]$ and t is the time in $[s]$. The initial condition is any velocity field that satisfies the continuity equation.

The source term is defined in all domain Ω_{PeD} (Fig. 3), but has values different from zeros only the lagrangean points coincide with the eulerian collocation points, *i.e.*, in Γ_{PhD} and Γ_i of the Fig. 3). Equation 3 enables the eulerian field perceives the presence of a solid interface (Enriques-Remigio and Silveira-Neto, 2007).

$$f_i(\vec{x}, t) = \begin{cases} F_i\left(\vec{X}, t\right) & \text{if} \quad \vec{x} = \vec{X} \\ 0 & \text{if} \quad \vec{x} \neq \vec{X} \end{cases}, \tag{3}$$

where $\vec{x}$ is the position of a fluid particle and $\vec{X}$ is the position of a fluid particle that is placed besides of the solid interface.

Equation 3 shows that the field $f_i(\vec{x}, t)$ is discontinuous, which can be numerically solved only when there is coincidence between the points that compose the interface domain with some collocation points that compose the fluid domain.

However when the problem has a non cartesian geometry, a distribution and interpolation functions must be used. Then the lagrangian force field, $F_i(\vec{X}, t)$, is calculated and can be distributed to eulerian domain, these functions can be found in Griffith and Peskin (2005).
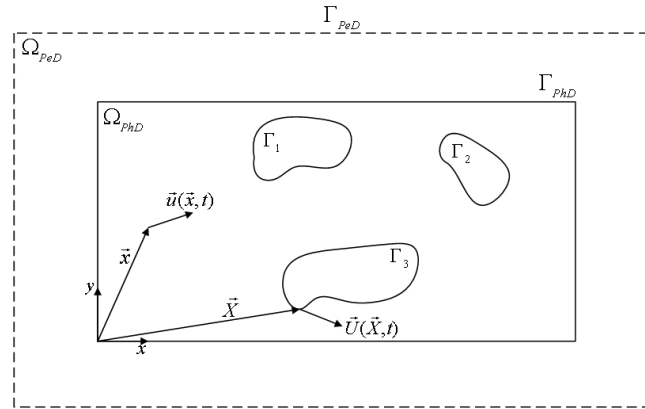

Figure 3. Schematically representation of eulerian and lagrangian domain.

2.2 Mathematical model for the immersed interface

The lagrangian force field is calculated by direct forcing methodology, which was proposed by Uhlmann (2005). One of the characteristics of this model is that we don't need to use ad-hoc constants. It allows the modeling of no-slip condition on immersed interface. The lagrangian force $F_i\left(\vec{X}, t\right)$ is given solving the momentum equation, Eq. 1, over the fluid-solid interface:

$$F_i\left(\vec{X}, t\right) = \frac{\partial U_i}{\partial t}\left(\vec{X}, t\right) + \frac{\partial}{\partial X_j}(U_i U_j)\left(\vec{X}, t\right) + \frac{\partial P}{\partial X_i}\left(\vec{X}, t\right) - \nu \frac{\partial^2 U_i}{\partial X_j \partial X_j}\left(\vec{X}, t\right). \tag{4}$$

The capital symbols are the same as Eq. 1, but they are calculated only over the lagrangian interface Γ shown in Fig. 3.

Using the temporal parameter, U^*, proposed by Wang *et al.* (2008) and discretizing the time operator, we have:

$$F_i\left(\vec{X}, t\right) = \frac{U_i\left(\vec{X}, t + \Delta t\right) - U_i^*\left(\vec{X}, t\right) + U_i^*\left(\vec{X}, t\right) - U_i\left(\vec{X}, t\right)}{\Delta t} + RHS_i\left(\vec{X}, t\right), \tag{5}$$

where Δt is the time step and

$$RHS_i\left(\vec{X}, t\right) = \frac{\partial}{\partial X_j}(U_i U_j)\left(\vec{X}, t\right) + \frac{\partial P}{\partial X_i}\left(\vec{X}, t\right) - \nu \frac{\partial^2 U_i}{\partial X_j \partial X_j}\left(\vec{X}, t\right). \tag{6}$$

The Eq. 5 is solved by decomposition the Eqs. 7 and 8:

$$\frac{U_i^*\left(\vec{X}, t\right) - U_i\left(\vec{X}, t\right)}{\Delta t} + RHS_i\left(\vec{X}, t\right) = 0, \tag{7}$$

$$F_i\left(\vec{X}, t\right) = \frac{U\left(\vec{X}, t + \Delta t\right) - U_i^*\left(\vec{X}, t\right)}{\Delta t}, \tag{8}$$

where $U\left(\vec{X}, t + \Delta t\right) = U_{FI}$ is the immersed boundary velocity, and $U_i^*\left(\vec{X}, t\right)$ is given by:

$$U_i\left(\vec{X}, t\right) = \begin{cases} u_i^*\left(\vec{X}, t\right) & \text{if} \quad \vec{x} = \vec{X} \\ 0 & \text{if} \quad \vec{x} \neq \vec{X} \end{cases}. \tag{9}$$

Equation 7 is solved at the eulerian domain at Fourier spectral space, *i.e.*, it is replaced by solution of the transformed Eq. 1 with $f_i = 0$. $u_i^*(\vec{x}, t)$ is interpolated for lagrangian domain, giving $U_i^*\left(\vec{X}, t\right)$ and it is computed on Eq. 8. Then it is smeared to eulerian collocation points. Finally, the eulerian velocities are updated by Eq. 10:

$$u_i\left(\vec{x}, t + \Delta t\right) = u_i^*\left(\vec{x}, t\right) + \Delta t f_i. \tag{10}$$

2.3 Mathematical model for the fluid in Fourier spectral space

Given the equations that govern the flow through immersed boundary method, the next step is to transform them to the Fourier spectral space. For instance, Fourier transform of continuity Eq. 2, gives:

$$\iota k_j \widehat{u}_j = 0, \tag{11}$$

where "^" means that variable is in Fourier spectral space. The Fourier transformation is performed using the FFT algorithm implemented by Takahashi (2006).

Equation 11 defines the wave number vector k_i is orthogonal to transform velocity, $\widehat{u}_i(\vec{k}, t)$. We can define the plane of divergence free, named plane π. It is perpendicular to wave number vector and thus, transformed velocity belongs to the plane π. By applying the Fourier transform in the momentum equation Eq. 1:

$$\frac{\partial \widehat{u}_i^*}{\partial t} + \iota k_j \widehat{u_i^* u_j^*} = -\iota k_i \widehat{p} - \nu k^2 \widehat{u}_i^*, \tag{12}$$

where k^2 is the square norm of the wave number vector, *i.e.* $k^2 = k_j k_j$.

By definition of the plane π, each of the terms of Eq. 12 assume a position related to it: the transient term $\frac{\partial \widehat{u}_i^*}{\partial t}$ and the viscous term $\nu k^2 \widehat{u}_i^*$ belong to the plane π. The gradient pressure term is perpendicular to plane π. The direction of non-linear term $\iota k_j \widehat{u_i^* u_j^*}$, a priori, is not known, when compared with the plane π. By joining the terms of Eq. 12, we found that:

$$\underbrace{\left[\frac{\partial \hat{u}_i^*}{\partial t} + \nu k^2 \hat{u}_i^*\right]}_{\in \pi} + \underbrace{\left[\iota k_j \widehat{u_i^* u_j^*} + \iota k_i \hat{p}\right]}_{\in \pi} = 0. \tag{13}$$

The Eq. 13 imply that:

$$\left[\iota k_j \widehat{u_j^* u_i^*} + \iota k_i \widehat{p}\right] = \wp_{im} \left[\iota k_j \widehat{u_m^* u_i^*}\right], \tag{14}$$

where $\wp_{ij}$ is the projection tensor (Canuto *et al.*, 2006).

The gradient pressure field is orthogonal to the plane π. So, the pressure and velocities fields at Fourier space are not coupled anymore. Nevertheless the pressure field can be recovered as a pos-processing procedure, as shown by (Mariano *et al.*, 2010).

Other important point is the non-linear term, which appears product of transformed functions, in agreement with Fourier transformed properties, this operation is a convolution product and its solution is given by convolution integral, this is solved by pseudo-spectral Fourier method, Canuto *et al.* (2007). Therefore the momentum equation in the Fourier space, using the projection method, assumes the following form:

$$\frac{\partial \hat{u}_i^* \left(\vec{k}, t\right)}{\partial t} + \nu k^2 \hat{u}_i^* \left(\vec{k}, t\right) = -\iota k_j \wp_{im} \int_{\vec{k} = \vec{r} + \vec{s}} \hat{u}_m^* \left(\vec{r}, t\right) \hat{u}_i^* \left(\vec{k} - \vec{r}, t\right) d\vec{r}. \tag{15}$$

The non-linear term can be handed by different forms: advective, divergent, skew-symmetric or rotational (Canuto *et al.*, 2007), in spite of being the same mathematically, they present different properties when discretized. The skew-symmetric form is more stable and present best results. Therefore, this procedure is used in the present work. The non-linear term is solved using the pseudo-spectral method (Canuto *et al.*, 2007). The velocity product is calculated at physical space and transformed to the spectral space.

2.4 Proposed Methodology: IMERSPEC

The proposed algorithm is described as:

1) Solve Eq. 14 in the Fourier spectral space and obtain the temporal parameter $\widehat{u^*}_i(\vec{k}, t)$, using the low dispersion and low storage Runge-Kutta method, proposed by Allampalli *et al.* (2009);

2) Use the Inverse Fast Fourier Transformer in $\widehat{u^*}_i(\vec{k}, t)$ and obtain $u_i^*(\vec{x}, t)$ at physic space;

3) Interpolate $u_i^*(\vec{x}, t)$ to the Lagrangian domain using Eq. 9;

4) Calculate the Lagrangian force, $F_i^*(\vec{X}, t)$, by Eq. 8;

5) Calculate the eulerian force, $f_i^*(\vec{x}, t)$ using Eq. 3;

6) Update the eulerian velocity, $u_i(\vec{x}, t + \Delta t)$ by Eq. 10 and transform it using FFT for spectral space, obtaining $\widehat{u}_i(\vec{x}, t + \Delta t)$, and return to step 1.

3. Results

Figure 4 shows the physical domain Ω_{PhD}, (solid line), that is immersed in periodical domain Ω_{PeD} (dashed line). The physical domain is no periodical and is bounded by immersed boundary Γ_{PhD}. The periodical domain is delimited by Γ_{PeD} boundary.

The Γ_{PhD} represent the "physic boundary conditions", *e.g.*, For the wall case, the no-slip boundary conditions in the upper and bottom walls and a inlet are imposed. In the outlet Γ_{PeD} and Γ_{PhD} are coincident, where periodical boundary conditions is used. In the entire Γ_{PeD} periodical boundary conditions are used too.
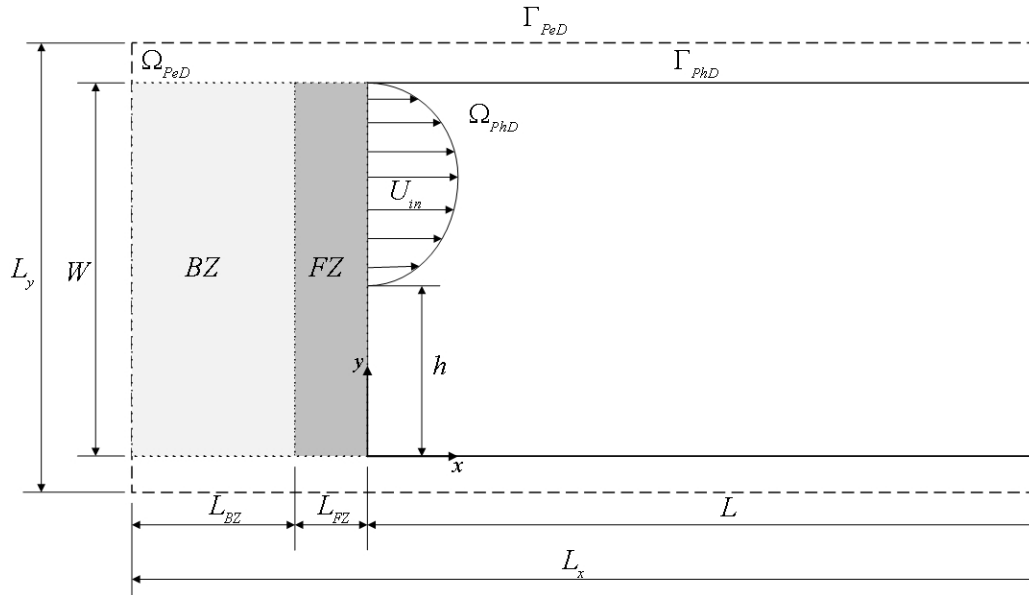

Figure 4. Backward-facing step immersed in general cartesian and periodic domain Ω_{PeD}.

The periodical boundary condition given in outlet make that the physical instabilities that leave the domain are reinjected in the inlet of the domain. In order to avoid that instabilities affect the forced boundary conditions at Γ_{PhD} we use a buffer zone (zone BZ in Fig. 4) in order to diffuse the vortex. The forcing zone (zone FZ in Fig. 4) is used to align the streamlines at the entrance.

In forcing zone, FZ, the procedure consists enforce the inlet profile using the immersed boundary methodology. In the present paper this inlet profile is provided by Lee and Mateescu (1998) and is given by Eq. 16. This velocity profile corresponds to a developed flow in a duct which mean velocity $U_\infty = 1.0\ [m/s]$.

$$U_{in}(y) = \begin{cases} 0 & \text{if} \quad 0 \leq y \leq h \\ -24(W - y)(h - y) & \text{if} \quad h < y \leq W \end{cases}. \tag{16}$$

The buffer function used in the present work was proposed by Joslin *et al.* (1991), Eq. 17. This function is used to drive the flow in a smooth way through the forcing zone:

$$BZ_i = \phi(x)\left(Q_i - Q_i^{ta}\right), \tag{17}$$

where Q_i^{ta} is the target solution; Q_i is the obtained Navier-Stokes solution; and the stretching function ϕ, is given by Eq. 18:

$$\phi = \frac{1}{2}\left[1 - \tanh\left(4 - 8\frac{x_{sB} - x}{x_{sB} - x_{fB}}\right)\right], \tag{18}$$

where x_{sB} and x_{fB} are the start and the final positions the buffer zone, respectively.

The BZ_i term given in Eq. 17, is transformed to Fourier spectral domain, obtaining $\widehat{BZ}_i$. This term is projected over the plane π and superimposed on the estimated velocity field, $\widehat{u^*}_i(\vec{k}, t)$:

$$\widehat{u^*}_i(\vec{k}, t) \leftarrow \widehat{u^*}_i(\vec{k}, t) - \widehat{BZ}_i(\vec{k}, t). \tag{19}$$

All simulations presented in this paper use the Runge-Kutta $RK46$ temporal integration, presented by Allampalli *et al.* (2009). The time step, Δt changes according to CFL criterium (Courant *et al.* (1967)).

3.1 Flow over a backward-facing step at $Re_h = 400$

In order to validate the methodology, flow simulations of a backward-facing step was carried out using the domain shown in Fig. 4. The domain dimensions are normalized by the step high $h = 0.5\ [m]$, $Lx/h = 73.14$ and $Ly/h = 2.29$. They were divided in $Nx = 2048$ and $Ny = 64$ collocation points, respectively. The aspect ratio is $W/h = 2.0$; $L_{BZ}/h = 3.73$ and $L_{FZ}/h = 0.53$.

The kinematic viscosity is given by $\nu = U_\infty h/Re_h\ [m^2/s]$, where the Reynolds number is taken as $Re_h = 400$ and U_∞ is the reference velocity, given by the mean velocity profile $U_{in}(y)$ (Eq. 16), *i.e.*, $U_\infty = 1.0\ [m/s]$. The target solution in buffer zone (Eq. 17) is the inlet velocity profile given by Eq. 16, *i.e.*, $Q_x^{ta} = U_{in}(y)$ inflow direction and $Q_y^{ta} = 0$ for vertical direction.

Figure 5 the streamlines were shown after the steady regime is attained over the full domain, including the buffer and forcing zones. In Fig. 6 a zoom over the recirculation zone of the Fig. 5 is shown. We note the two recirculations provided by the boundary layer detachment. This results is in agreement with what is expected for this flow.
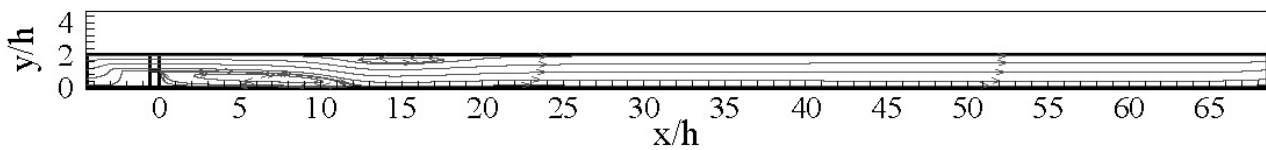

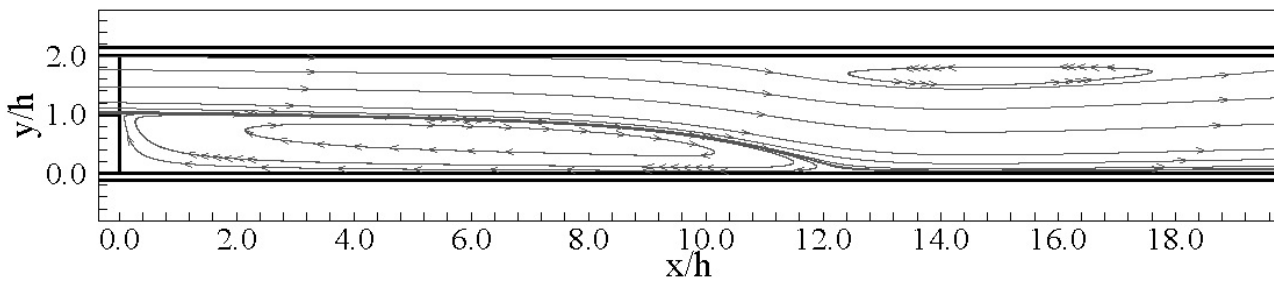Figure 5. Streamlines of the flow over backward-facing step at $Re_h = 400$ in $tU_\infty/h = 400$.

Figure 6. Details of streamlines of the flow backward-facing step at $Re_h = 400$ in $tU_\infty/h = 400$.

Vis-a-vis to demonstrate the importance of the buffer and forcing zones Fig. 7 shows how the fluid particles are driven to the entrance of the physical domain Ω_{PhD}. Figure 7 (a) shows the streamlines for the case with forcing zone where we can see that they are parallels to the walls, as it must happen at a wind tunnel.
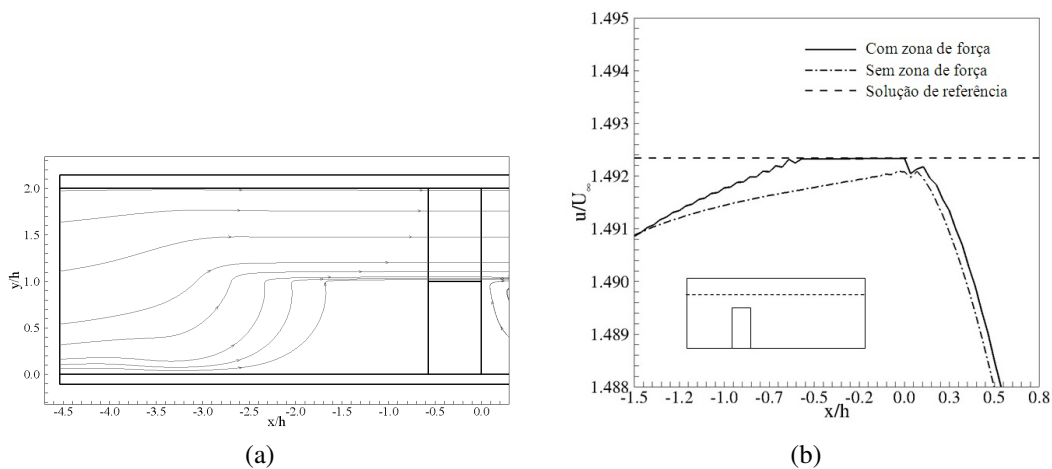

(a)

(b)

Figure 7. Details of streamlines over the buffer zone (a); profile of horizontal velocity component at y/h=1.49 (b); at $Re_h = 400$ and $tU_\infty/h = 400$.

Figure 7 (b) shows the streamwise velocity component values, at $y/h = 1.49$, obtained with and without the forcing zone. This figure shows also a reference solution or the target velocity, which is given by Eq. 16. We see that the streamlines becomes parallels as long as the fluid entry in the forcing zone, and find the target velocity field used as the reference to calculate the force profile given by Eq. 16. Without forcing zone, the velocity at the entrance plane doesnŠt

reach the target velocity value and is not parallel to the walls. The oscillation that appears after $x/h = 0.0$ is already inside the domain and is the result of the first physical instabilities, like Kelvin-Helmholtz.

3.1.1 Different Reynolds numbers

In this section we use the same settings of last section. However we set different Reynolds numbers for flow simulation of backward-facing step. The Fig. 8 shown the vorticity component in z direction for four Reynolds numbers, ($Re_h = 200, 800, 1500$ and 6000). We note that the flow at $Re_h = 200$ is stable in all the domain. At $Re_h = 800$ and $Re_h = 1500$ the flow become unstable after the recirculation zone passing through a transition zone. In this range of the Reynolds number it is possible to note the vortex counterclock-wise alternately between the upper and bottom walls. At $Re_h = 6000$ the behavior of flow become unstable in all the domain.
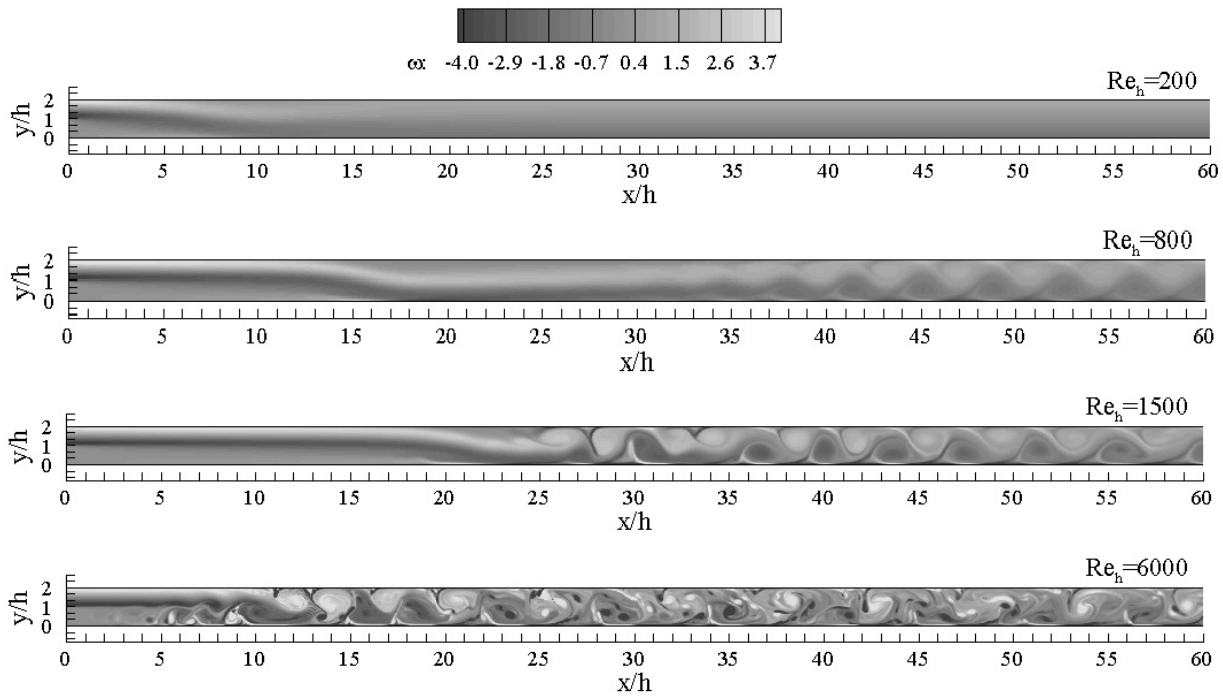

Figure 8. Component vorticity in z direction (ω_z) for different Reynolds numbers in $tU_\infty/h = 400$.

In order to validate the methodology we compare the results of inferior reattachment point, x_r/h, with experimental work of Lee and Mateescu (1998). The results of this comparison are presented in Tab. 1, where a good agreement up to $Re_h = 400$ is presented. As already shown by Armaly *et al.* (1983), this effect was expected, because the simulations are two-dimensional. By increasing the Reynolds number the three dimensional effects become important.

Table 1. Comparison of mean position of reattachment point, x_r/h, for different Reynolds number.

Re_h	Lee and Mateescu (1998)	Present work
200	8.30	8.50
250	9.10	9.71
300	10.30	10.64
350	11.10	11.39
400	12.90	12.18
450	13.20	12.61
500	15.50	13.50

3.2 Flow over three-dimensional backward-facing step

The present section provides two important results. First the extension to third dimension of the methodology IMER-SPEC and the parallel algorithm is straightforward. Second it shows that three dimensional effects are very important as the Reynolds number is increased.

A simulation of flow over backward-facing step was performed at $Re_h = 400$ with dimensions $h = 0.5$ $[m]$, $L_x/h = 54.86$, $L_y/h = 2.29$ and $L_z/h = 2.29$ divided in $N_x = 768$, $N_y = 32$ and $N_z = 32$ collocation points, respectively. The aspect ratio is $W/h = 2.0$; $L_{BZ}/h = 3.60$ and $L_{FZ}/h = 0.70$ (Fig. 4). The boundary conditions in spawnwise direction are periodicals and the planes of forcing zone is given by Eq. 16. In order to model the physical noise that has in experimental setup (Smirnov *et al.*, 2001), random perturbations (order of $10^{-4}U_\infty$) are imposed on the inlet plane over the velocity field. In order to avoid the Gibbs phenomenon a sharpened raised cosine present in Canuto *et al.* (2006) is used for each time step over the velocity fields.

A simulation at $Re_h = 400$, using $CFL = 0.5$ was performed. The results are presented in Fig. 9 and are compared with experimental profiles of Lee and Mateescu (1998). It is also compared with the two-dimensional results of present work. Table 2 show the reattachment point on the inferior wall, x_r/h. The detachment point x_s/h and the reattachment point x_{rs}/h on the superior wall are also presented.
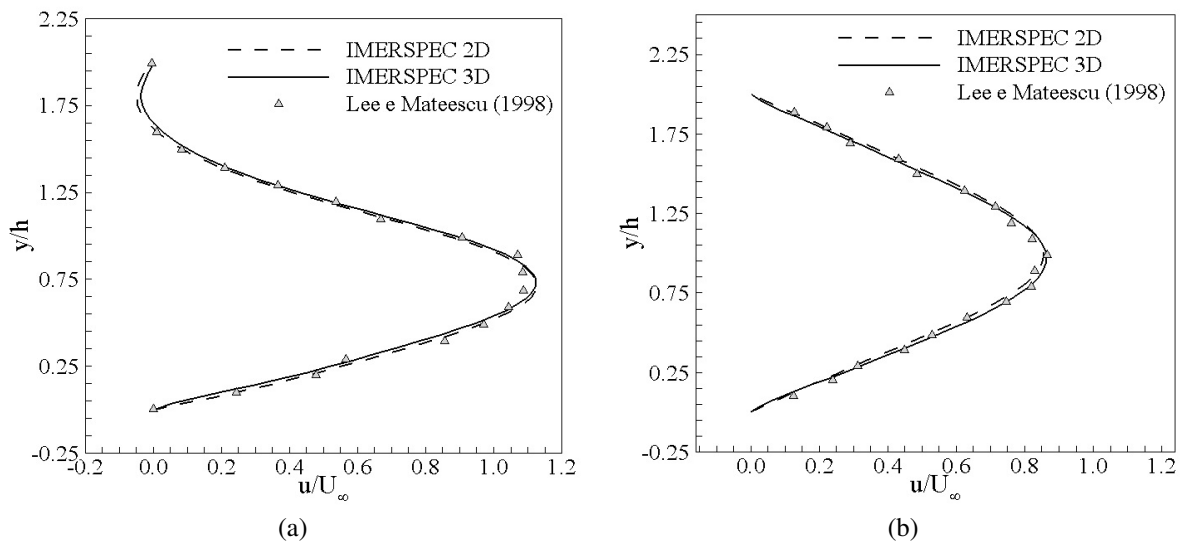

Figure 9. Longitudinal component velocity profiles at $tU_\infty/h = 100.0$ in (a) $(x/h; z/h) = (7.0; 1.0)$ and (b) $(x/h; z/h) = (15.0; 1.0)$. Comparison with experimental results of Lee and Mateescu (1998) and two-dimensional results of present work.

We can note in Fig. 9 that three-dimensional results are in good agreement with experimental profiles of Lee and Mateescu (1998). The comparison of two-dimensional results of the present paper are very closed, since the backward-facing step at $Re_h = 400$ is stable and physically the flow is two-dimensional.

Table 2. Comparison of position of reattachment point on the inferior wall x_r/h; the detachment point on the superior wall x_s/h; and detachment point on the superior wall, x_{rs}/h, for the backward-facing step flow at $Re_h = 400$.

Works	x_r/h	x_s/h	x_{rs}/h
IMERSPEC 2D	12.16	10.12	20.51
IMERSPEC 3D	11.70	11.30	19.10
Experimental Lee and Mateescu (1998)	12.90	10.30	20.50

A simulation of backward-facing step flow at $Re_h = 1000$ was performed with $h = 0.5$ $[m]$, $L_x/h = 54.86$, $L_y/h = 2.29$ and $L_z/h = 4.30$, divided in $N_x = 768$, $N_y = 32$ and $N_z = 32$ collocation points, respectively. The aspect ratio is $W/h = 2.0$; $L_{BZ}/h = 3.60$ and $L_{FZ}/h = 0.70$ (Fig. 4). Fig. 10 shown the z vorticity component in different planes.

In Fig. 10 (a) we can see the Kelvin-Helmoltz instabilities that are generated after reattachment point, x_r/h. In Fig. 10 (b) is possible to note the oscillations in spanwise direction, show the three-dimension features of backward-facing step flow at $Re_h = 1000$ and the transition to turbulence. We observed the recirculation zone generated by adverse gradient of pressure in Fig. 10 (c).

In Tab. 3 a comparison of mean positions of reattachment point of inferior wall (x_r), detached point of superior wall (x_s) and the reattached point of superior wall (x_{rs}) with experimental results of Lee and Mateescu (1998) and the two-dimensional results of the present work is given.

The results of two-dimensional simulations (IMERSPEC 2D) of backward-facing step flow at $Re_h = 1000$ presented in Tab. 3 are not in good agreement with experimental data. On the other hand, the results of IMERSPEC 3D are very closed of Lee and Mateescu (1998) results, shown the importance of the three-dimensional effects.
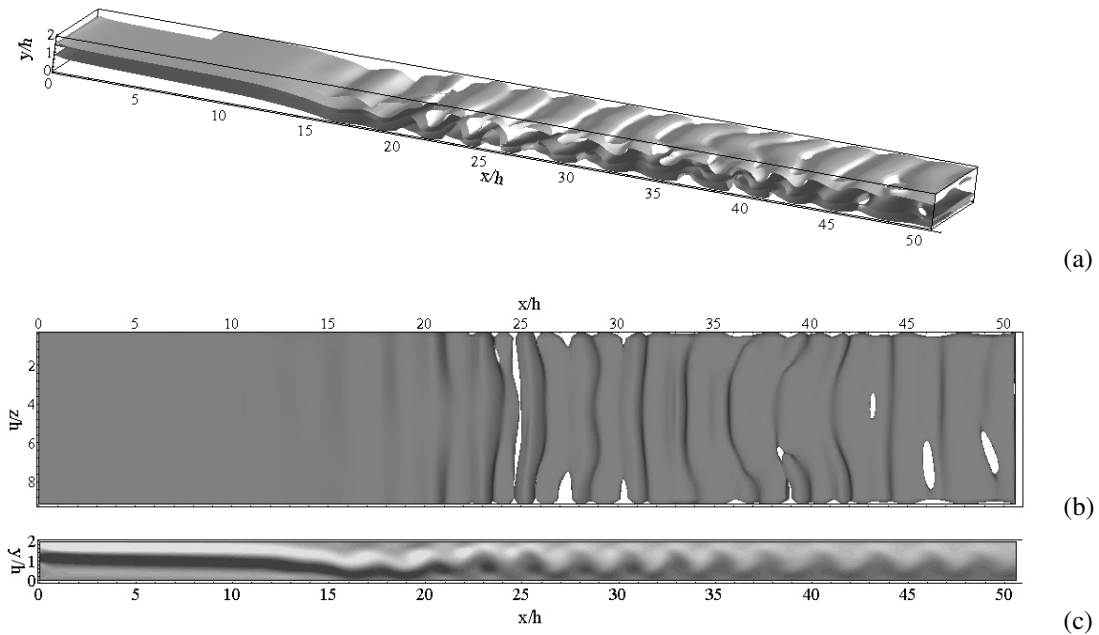
(a)

(b)

(c)

Figure 10. Backward-facing step flow at $Re_h = 1000$ and $tU_\infty/h = 100.0$. (a) Iso-surface of vorticity spanwise component $\omega_z = -1.0$ (black) and $\omega_z = 1.0$ (white); (b) Iso-surface of vorticity spanwise component $\omega_z = -1.0$; (c) Vorticity spanwise component at z center plane $-1.0 < \omega_z < 1.0$.

Table 3. Comparison of position of reattachment point on the inferior wall x_r/h; the detachment point on the superior wall x_s/h; and detachment point on the superior wall, x_{rs}/h, for the backward-facing step flow at $Re_h = 1000$.

Works	x_r/h	x_s/h	x_{rs}/h
IMERSPEC 2D	18.10	15.15	36.09
IMERSPEC 3D	12.42	16.31	19.36
Experimental Lee and Mateescu (1998)	12.80	9.70	18.40

4. CONCLUSIONS

The very complex flows over a backward-facing step were chosen. Two dimensional and three dimensional simulations were done and results were compared with experimental and with numerical results of others authors. Very good agreement was obtained for two-dimensional simulations up to $Re_h = 400$ and at $Re_h = 1000$ only the three-dimensional results are in agreement with the experimental data, showing the existence of three-dimensional effects of turbulence transition. We consider the proposed methodology very promising to solve complex flows.

It is important to note that IMERSPEC methodology was developed to incompressible flows and provide good features for Navier-Stokes solutions, as well as high accuracy and high convergence rates. Furthermore, CPU time should be less than high order methodologies in physical space. This is because the pressure linear solver for Poisson equation is replaced by product of vector-matrix, providing by Fourier pseudo-spectral method.

5. ACKNOWLEDGEMENTS

6. REFERENCES

Allampalli, V., Hixon, R., Nallasamy, M. and Sawyer, S., 2009. "High-accuracy large-step explicit runge - kutta ($hale - rk$) schemes for computational aeroacoustics". *Journal of Computational Physics*, Vol. 228, pp. 3837–3850.

Armaly, B., Durst, F., Pereira, J. and Schonung, B., 1983. "Experimental and theoretical investigation of backward-facing step flow". *Journal of Fluid Mechanics*, Vol. 127, pp. 473–496.

Canuto, C., Hussaini, M.Y., Quarteroni, A. and Zang, T.A., 2006. *Spectral methods: fundamentals in single domains*. Spriger Verlag, New York.

Canuto, C., Hussaini, M.Y., Quarteroni, A. and Zang, T.A., 2007. *Spectral methods: evolution to complex geometries and applications to fluid dynamics*. Spriger Verlag, New York.

Courant, R., Friedrichs, K. and Lewy, H., 1967. "On the partial difference equations of mathematical physics". *IBM Journal*, Vol. 1, pp. 215–234.

Eaton, J.K. and Johnston, J.P., 1980. "Turbulent flow reattachment: an experimental study of the flow and structure behind a backward-facing step". Technical Report Rept. MD-39, Thermosciences Division, Department of Mechanical Engineering, Stanford University, Thermosciences Division, Department of Mechanical Engineering, Stanford University, Palo Alto.

Enriques-Remigio, S. and Silveira-Neto, A., 2007. "A new modeling of fluid-structure interaction problems through immersed boundary method/virtual psysical model (ibm/vpm)". In *Congresso Brasileiro de Engenharia Mecânica, 19*. ABCM, Brasília. 1 CD-ROM.

Gartling, D., 1990. "A test problem for outflow boundary conditions - flow over a backward-facing step". *International Journal of Numerical Methods in Fluids*, Vol. 11, pp. 953–967.

Goldstein, D., Adachi, T. and Sakata, H., 1993. "Modeling a no-slip flow with an external force field". *Journal of Computational Physics*, Vol. 105, pp. 354–366.

Griffith, B.E. and Peskin, C.S., 2005. "On the order of accuracy of the immersed boundary method: Higher order convergence rates for sufficiently smooth problems". *Journal of Computational Physics*, Vol. 208, pp. 75–105.

Joslin, R.D., Streett, C.L. and Chang, C.L., 1991. "Validation of 3d incompressible spatial direct numerical simulation. code a comparison with linear stability and parabolic stability equation theories for boundary layer transition on a flat plate". Technical report, Langley Research Center - NASA. (Report NASA, v. 3205).

Le, H., Moin, P. and Kim, J., 1997. "Direct numerical simulation of turbulent flow over a backward-facing step". *Journal of Fluids Mechanics*, Vol. 330, pp. 349–374.

Lee, T. and Mateescu, D., 1998. "Experimental and numerical investigation of 2-d backward-facing step flow". *Journal of Fluids and Structures*, Vol. 12, pp. 703–716.

Mariano, F.P., Moreira, L.Q., Silveira-Neto, A., da Silva, C.B. and Pereira, J.C.F., 2010. "A new incompressible navier-stokes solver combining fourier pseudo-spectral and immersed boundary method". *Computer Modeling in Engineering Science*, Vol. 59, pp. 181–216.

Silveira-Neto, A., Grand, D., Metais, O., Gonze, M. and Lesieur, M., 1993. "A numerical investigation of the coherent vortices in turbulence behind a backward-facing step". *Journal of Fluid Mechanics*, Vol. 256, pp. 1–25.

Smirnov, A., Shi, S. and Celik, I., 2001. "Random flow generation technique for large eddy simulations and particle-dynamics modeling". *Journal of Fluids Engineering*, Vol. 123, pp. 359–371. doi:DOI: 10.1115/1.1369598.

Takahashi, D., 2006. "A hybrid mpi/openmp implementation of a parallel 3-d fft on smp clusters". *Lecture Notes in Computer Science*, Vol. 3911, pp. 970–977.

Uhlmann, M., 2005. "An immersed boundary method with direct forcing for the simulation of particulate flows". *Journal of Computational Physics*, Vol. 209, pp. 448–476.

Wan, D. and Turek, S., 2007. "An efficient multigrid-fem method for the simulation of solid-liquid two phase flows". *Journal of Computational and Applied Mathematics*, Vol. 203, pp. 561–580.

Wang, Z., Fan, J. and Luo, K., 2008. "Combined multi-direct forcing and immersed boundary method for simulating flows with moving particles". *International Journal of Multiphase Flow*, Vol. 34, pp. 283–302.

7. Responsibility notice

The authors are the only responsible for the printed material included in this paper